An integrated data-driven approach to seismic reflection imaging

Thomas Hertweck, Christoph Jäger, Jürgen Mann & Eric Duveneck
Geophysical Institute, University of Karlsruhe, Germany

Summary

The development of new seismic reflection imaging methods is an area of ongoing research. With increasing technical and computational resources, powerful alternatives to the conventional methods like, e. g., the NMO/DMO/stack approach, evolved in recent years. Among these new methods is, for instance, the data-driven simulation of zero-offset (ZO) sections by means of the Common-Reflection-Surface (CRS) stack. With the kinematic wavefield attributes derived during this process, an entire integrated seismic reflection imaging work flow can be established that includes the CRS stack itself, and the use of the wavefield attributes to estimate a velocity model and to optimize the subsequent depth migration. Here, we demonstrate some of the possibilities on a synthetic data example.

Introduction

Seismic reflection data processing aims at obtaining the best possible structural image of the subsurface, either in the time or in the depth domain. Especially in regions with complex geological structures, this is a challenging task for geoscientists and their processing tools and requires to combine all available geological and geophysical information. In recent years, data-driven imaging methods have increasingly gained in relevance. They open up a number of possibilities in seismic data processing. Here, we want to focus on the Common-Reflection-Surface (CRS) stack and its integration into the seismic reflection imaging work flow. A general overview of the main data processing steps is given in Figure 1.

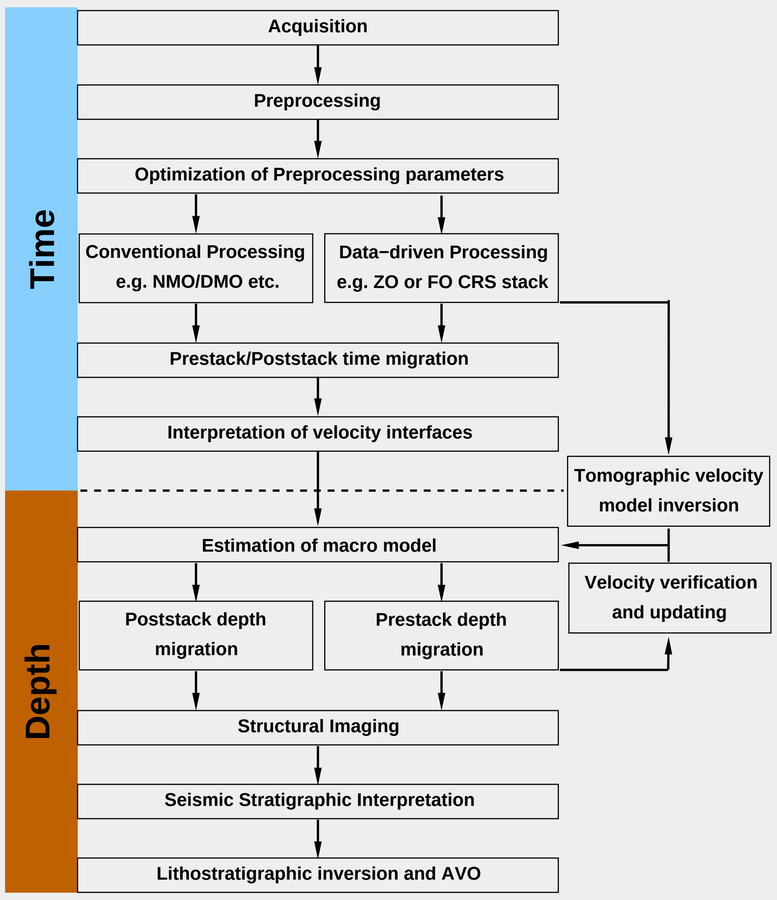

Figure 1: General seismic data processing flowchart, modified after Farmer et al. (1993).

As is shown below, the CRS stack produces, along with a simulated ZO section, several wavefield attribute sections that are useful in further processing:
Firstly, these attributes contain kinematic information that can be utilized in a tomographic velocity model inversion. This allows to obtain a smooth velocity model for depth imaging and, thus, helps to establish the link between the time and the depth domain. If required, this model can then be further refined by migration-based velocity analysis.
Secondly, the attributes can be used (in combination with the previously determined velocity model) in the depth migration process itself, e. g., to restrict the aperture of Kirchhoff migration operators to optimal values.
Following this approach, integrated pre- and post-stack processing strategies are available. They are based on flexible combinations of conventional, model-based technologies and emerging data-driven imaging methods.

The model setup

To illustrate the application of the CRS stack and the resulting CRS attribute sections, our approach has been applied to a synthetic multi-coverage data set. The data (only primary P-wave reflections, no diffractions) were modeled by ray tracing in the blocky model displayed in Figure 2, using a zero-phase wavelet with a dominant frequency of 20 Hz. The temporal sampling interval is 4 ms.

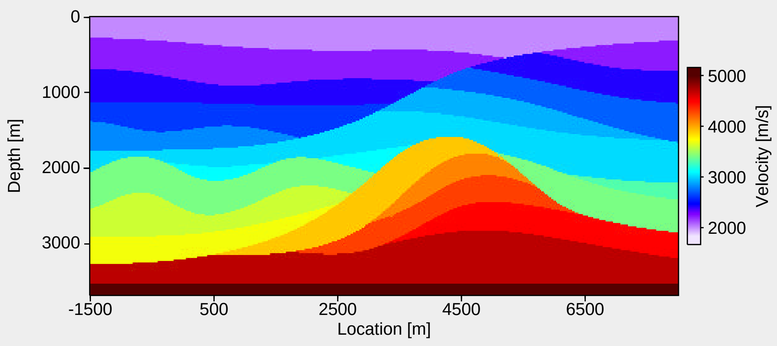

Figure 2: Synthetic blocky velocity model used to simulate a synthetic pre-stack data set. Denoted in color is the P-wave velocity.

A total of 600 shots with a spacing of 20 m and shot locations ranging from $x = -2000$ m to $x = 9980$ m were modeled. Each shot was recorded by 95 receivers with a regular spacing of 20 m, a minimum offset of 100 m and a maximum offset of 1980 m. The resulting CMP spacing is 10 m with a maximum of 48 traces per CMP location. Band-limited random noise was then added to the pre-stack data. The resulting common-offset section for the minimum occurring offset of 100 m is displayed in Figure 3a), while a CMP gather for the CMP location 2000 m is shown in Figure 3b). A number of hyperbolic reflection events is clearly visible.

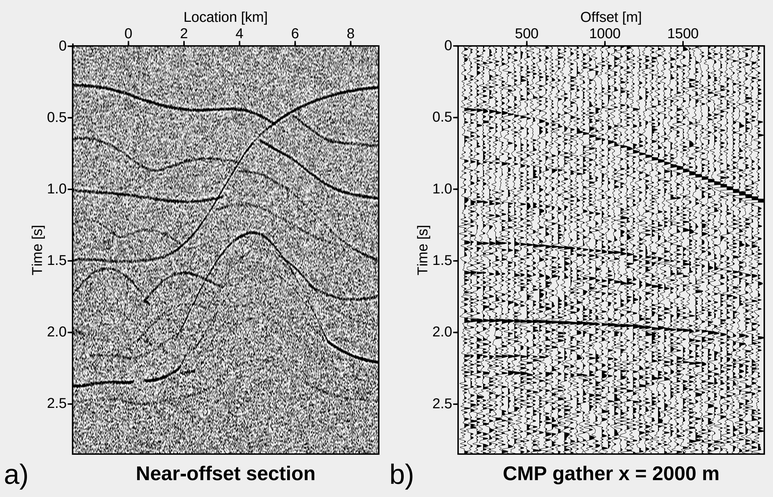

Figure 3: Synthetic data example: a) near-offset section extracted form the noisy pre-stack data set; b) CMP gather for midpoint location 2000 m. Diffraction events have not been modeled.

The Common-Reflection-Surface (CRS) stack

The Common-Reflection-Surface (CRS) stack (see, e. g., Müller, 1999; Jäger et al., 2001; Mann, 2002) was originally introduced to simulate high-quality ZO sections from pre-stack data. In contrast to conventional ZO simulation methods, the CRS approach fits entire stacking *surfaces* to the events rather than only stacking *trajectories*. Thus, far more traces contribute to a ZO sample to be simulated. The stacking operator for a ZO sample (t_0, x_0) reads

$$t^2(x_m, h) = \left[t_0 + \frac{2\sin\alpha\,(x_m - x_0)}{v_0}\right]^2 + \frac{2t_0\cos^2\alpha}{v_0}\left[\frac{(x_m - x_0)^2}{R_N} + \frac{h^2}{R_{NIP}}\right]$$

where the half-offset h and the midpoint x_m between source and receiver describe the acquisition geometry and v_0 is the near-surface velocity. The remaining three parameters are called kinematic wavefield attributes and describe the propagation direction (α) and wavefront curvatures (R_{NIP}, R_N) of two hypothetical experiments observed at $(z = 0, x_m)$. The NIP (normal incidence point) wave is the hypothetical wave that would be obtained by placing a point source at the NIP of the ZO ray.

To determine the attributes of the CRS operator fitting best an actual reflection event, a coherence analysis is performed along stacking operators in the pre-stack data with different sets of kinematic wavefield attributes. The best fitting operator yields the highest coherence. This analysis is repeated for each ZO sample to be simulated, irrespective whether there is an actual reflection event. Thus, the entire CRS approach can be applied in a non-interactive way and without the need for any a priori knowledge of a macro-velocity model.
An example of a CRS stacked ZO section simulated from the pre-stack data for the previously introduced model is shown in Figure 4, along with its associated coherence and kinematic wavefield attribute sections in Figure 5.

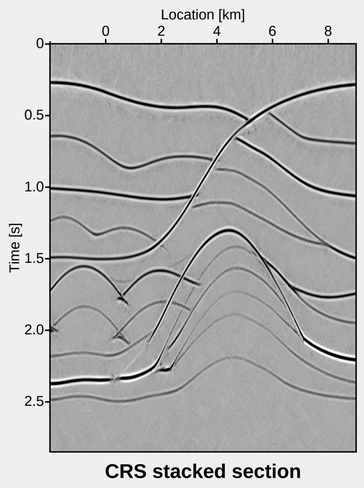

Figure 4: ZO section simulated by means of the CRS stack method. As expected, the S/N ratio is significantly increased, as compared to the unstacked near-offset section shown in Figure 3a).

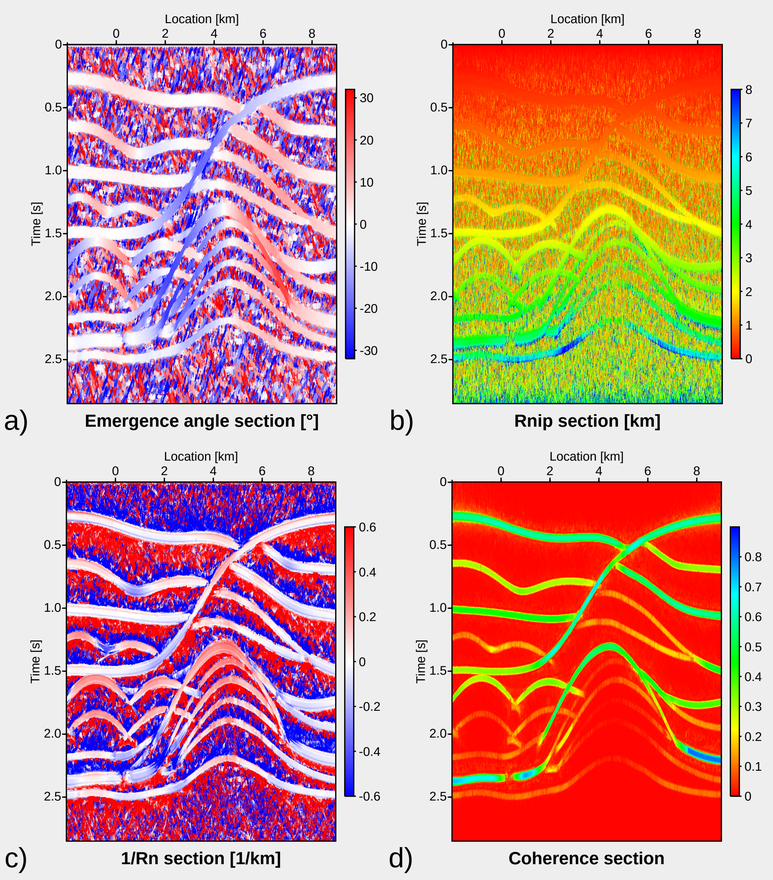

Figure 5: The additional CRS sections: a) emergence angle α section; b) section of the radius of curvature R_{NIP}; c) section of the curvature $K_N = 1/R_N$; d) coherence section.

The coherence section (Figure 5d)) shows the maximum semblance value obtained along the CRS operator for each simulated ZO sample. All CRS attribute sections only have meaningful values where the coherence value is sufficiently high, i. e., on actual reflection events. Figure 5a) shows the emergence angle section; the emergence angle varies roughly between -30° and +30°. The NIP wave curvature is displayed in Figure 5b). In a constant velocity medium the NIP wave radius of curvature would coincide with the normal ray length (i. e., the distance to the NIP). Figure 5c) shows the normal wave curvature.
The CRS stack has also been successfully applied to real data in 2D and 3D (see, e. g., Bergler et al., 2002; Trappe et al., 2001; Cristini et al., 2002).

An integrated data-driven approach to seismic reflection imaging

Thomas Hertweck, Christoph Jäger, Jürgen Mann & Eric Duveneck
Geophysical Institute, University of Karlsruhe, Germany

Velocity model estimation

The determination of a velocity model is one of the crucial steps in seismic depth imaging. Usually, stacking velocities are used for an initial velocity model. The model is then iteratively updated by repeated pre-stack migration and analysis of residual moveouts in common-image gathers. This is an expensive and time-consuming process.

As mentioned above, the CRS attributes R_{NIP} and α describe the emerging NIP wavefront at $(z = 0, x_{\mathrm{m}})$. The NIP wave can be used for the estimation of a velocity model for depth imaging. In a correct velocity model, the NIP wave radius, when propagated back into the subsurface, should shrink to zero at its hypothetical source location at zero traveltime. Based on this criterion, the CRS attributes R_{NIP} and α can be applied in a tomographic inversion approach by minimizing the difference between the measured and modeled values of the quantities characterizing the considered NIP waves (e. g., Duveneck and Hubral, 2002). The subsurface locations of the corresponding normal-incidence points and the local reflector orientations are obtained simultaneously with the velocity model.

In contrast to conventional reflection tomography, which has the drawback that it requires extensive and often difficult picking in the pre-stack data, the method applied here allows picking in a CRS stack section of significantly increased S/N ratio. Furthermore, as a smooth velocity model description is used, it is no longer necessary to pick continuous events over successive traces.

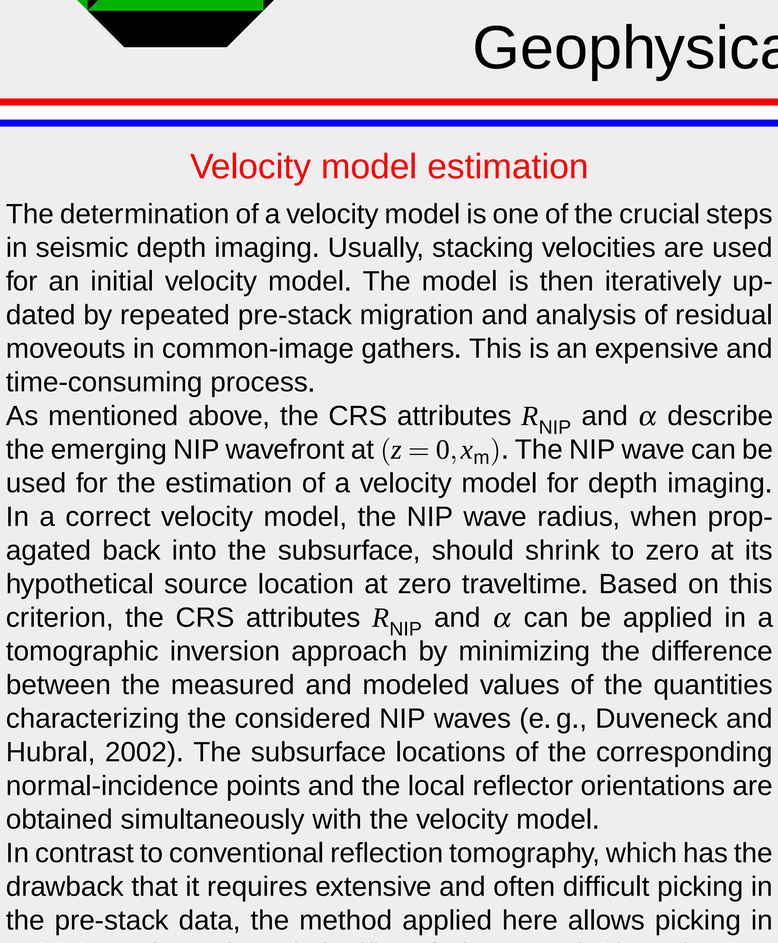

Figure 6: Inversion of the CRS wavefield attributes: a) reconstructed smooth velocity model; b) reconstructed model with reconstructed reflector elements; c) reconstructed reflector elements superimposed onto the true blocky model.

An example of the application of the CRS-stack-based tomographic velocity model estimation to the synthetic data shown previously is given in Figure 6a)-c). A total of 505 data points consisting of the values R_{NIP} and α at a number of locations (x_0, t_0) have been obtained from the corresponding sections (Figure 5a) and b). Figure 6a) shows the reconstructed velocity model (described by B-splines). In Figure 6b), the same smooth inversion result is shown together with the reflection point locations and local reflector dips (displayed as plane reflector elements) associated with the input data. The reconstructed model resembles a smoothed version of the true blocky velocity model (Figure 2). The reconstructed smooth model is kinematically correct, i. e., reflector elements fall into the correct subsurface locations. This can be seen when plotting the reconstructed reflector elements into the true model as was done in Figure 6c).

Depth migration

Apart from the migration velocity model obtained with the above described approach, ray-based migration processes themselves can benefit from the CRS attributes: Vieth (2001) used data-derived emergence angle information to increase the efficiency of depth migration. In general, it is possible to apply the attributes for a limited-aperture Kirchhoff depth migration where the stacking is then only performed in the vicinity of the stationary point within the projected Fresnel zone. This significantly reduces the computational costs and the migration noise while still allowing the correct handling of amplitudes (Schleicher et al., 1997; Sun, 2000). Figure 7a) shows a conventional (i. e., without applying CRS attributes) limited-aperture post-stack depth migration of the CRS stack section (Figure 4) using the reconstructed velocity model (Figure 6a)). Figure 7b) depicts the pre-stack depth migration result of the synthetic multicoverage data using the reconstructed velocity model. For a good approximation of the projected Fresnel zone in pre-stack migration, additional CRS attributes for the finite-offset case would be required. However, the finite-offset CRS stack was not performed for this example as our primary goal was to test the reconstructed velocity model. Figure 8 shows two selected common-image gathers. Obviously, most events are flat and no additional migration-based model refinement was applied. Thus, the reconstructed velocity model is kinematically consistent with the entire pre-stack data.

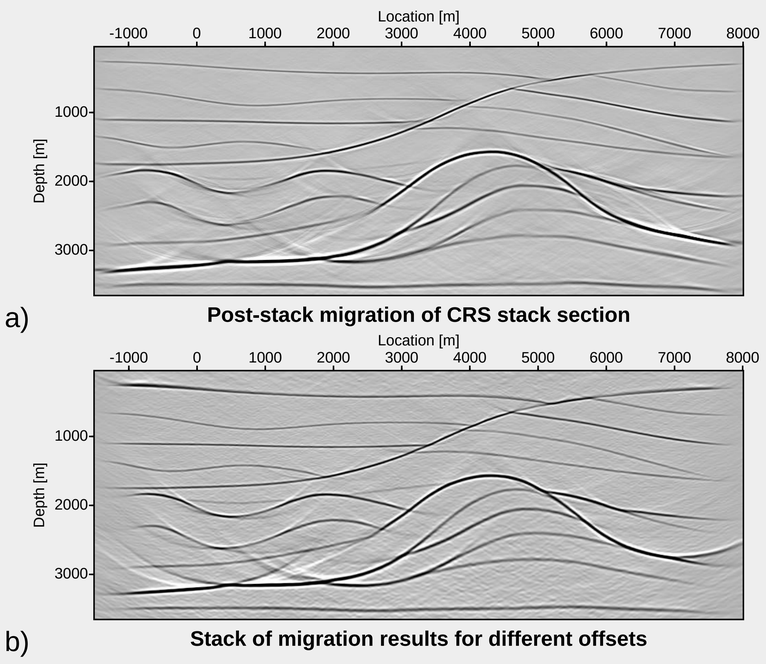

Figure 7: Depth migration results: a) post-stack depth migration of the CRS stack (Figure 4) section using the reconstructed velocity model (Figure 6a)); b) pre-stack depth migration using the reconstructed velocity model. The artifacts are due to shortcomings of the ray tracing modeling of the synthetic data.

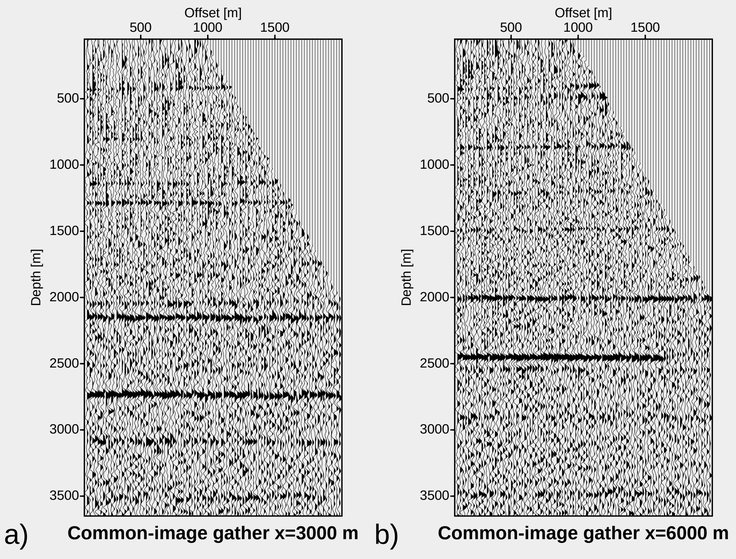

Figure 8: Common-image gathers a) at $x = 3000\,\mathrm{m}$ and b) at $x = 6000\,\mathrm{m}$, respectively. Most of the events are flat.

Acknowledgments

This work was kindly supported by the sponsors of the *Wave Inversion Technology (WIT) Consortium*, Karlsruhe, Germany.

Conclusions

We have demonstrated that the CRS stack and the associated kinematic wavefield attributes can be used in seismic imaging applications which go far beyond the purposes for which the method was originally designed—the simulation of ZO sections with significantly improved S/N ratio. The kinematic wavefield attributes contain information that can be used for the estimation of migration velocity models. In addition, they can be applied to determine projected Fresnel zones and increase the efficiency of Kirchhoff depth migrations. Apart from the applications discussed here, the CRS stack has potential in other seismic processing topics such as static corrections or redatuming, see also the section *Related presentations* below. Together with other recently developed extensions of the CRS stack (3D ZO CRS stack, 2D finite-offset CRS stack, and CRS stack allowing for topographic variations), imaging can be performed with a variety of case-specific strategies. In particular, data of poor quality, land data suffering from topography and near-surface effects, or data with irregular acquisition geometries are expected to benefit from this approach.

References

Bergler, S., Hubral, P., Marchetti, P., Cristini, A., and Cardone, G. (2002). 3D common-reflection-surface stack and kinematic wavefield attributes. *The Leading Edge*, 21(10):1010–1015.

Cristini, A., Cardone, G., and Marchetti, P. (2002). 3D zero-offset Common Reflection Surface Stack for land data – real data example. 64th Mtg. Eur. Assn. Geosci. Eng., Extended Abstracts.

Duveneck, E. and Hubral, P. (2002). Tomographic velocity model inversion using kinematic wavefield attributes. In *Expanded Abstracts*, pages 862–865. 72nd Ann. Internat. Mtg., Soc. Expl. Geophys.

Farmer, P., Gray, S., Hodgkiss, G., Pieprzak, A., Ratcliff, D., and Whitcombe, D. (1993). Structural Imaging: Toward a Sharper Subsurface View. *Oilfield Review*, 5(1):28–41.

Jäger, R., Mann, J., Höcht, G., and Hubral, P. (2001). Common-reflection-surface stack: Image and attributes. *Geophysics*, 66(1):97–109.

Mann, J. (2002). *Extensions and applications of the Common-Reflection-Surface Stack method*. Logos Verlag, Berlin.

Müller, T. (1999). *The Common Reflection Surface Stack Method – seismic imaging without explicit knowledge of the velocity model*. Der Andere Verlag, Bad Iburg.

Schleicher, J., Hubral, P., Tygel, M., and Jaya, M. S. (1997). Minimum apertures and fresnel zones in migration and demigration. *Geophysics*, 62(01):183–194.

Sun, J. (2000). Limited aperture migration. *Geophysics*, 65(2):584–595.

Trappe, H., Gierse, G., and Pruessmann, J. (2001). Case studies show potential of Common Reflection Surface stack - structural resolution in the time domain beyond the conventional NMO/DMO stack. *First Break*, 19(11):625–633.

Vieth, K.-U. (2001). *Kinematic wavefield attributes in seismic imaging*. PhD thesis, Universität Karlsruhe.

Related presentations

P007 Pulse stretch effects in the context of data-driven imaging methods, *Mann and Höcht*

D17 CRS imaging of 3-D seismic data from the active continental margin offshore Costa Rica, *Trappe et al.*

D18 Residual static correction by means of kinematic wavefield attributes, *Koglin and Ewig*

D27 Determination of velocity models from data-derived wavefront attributes, *Duveneck*

D31 3-D macro-velocity inversion by means of kinematic wavefield attributes, *Höcht et al.*